







Article

Bio-Synthesized Tin Oxide Nanoparticles: Structural, Optical, and Biological Studies

Salah Ud Din ¹, Sabah Hanif Kiani ¹, Sirajul Haq ^{1,*}, Pervaiz Ahmad ², Mayeen Uddin Khandaker ³,
Mohammad Rashed Iqbal Faruque ⁴, Abubakr M. Idris ^{5,6} and M. I. Sayyed ^{7,8}

¹ Department of Chemistry, University of Azad Jammu and Kashmir, Muzaffarabad 13100, Pakistan; salah.mahsud@ajku.edu.pk (S.U.D.); sabah.hanif555@gmail.com (S.H.K.)

² Department of Physics, University of Azad Jammu and Kashmir, Muzaffarabad 13100, Pakistan; pervaiz_pas@yahoo.com

³ Center for Applied Physics and Radiation Technologies, School of Engineering and Technology, Sunway University, Petaling Jaya 47500, Malaysia; mayeenk@sunway.edu.my

⁴ Space Science Centre (ANGKASA), Universiti Kebangsaan Malaysia, Bangi 43600, Malaysia; rashed@ukm.edu.my

⁵ Department of Chemistry, College of Science, King Khalid University, Abha 62529, Saudi Arabia; abubakridris@hotmail.com

⁶ Research Center for Advanced Materials Science (RCAMS), King Khalid University, Abha 62529, Saudi Arabia

⁷ Department of Physics, Faculty of Science, Isra University, Amman 11622, Jordan; dr.mabualssayed@gmail.com

⁸ Department of Nuclear Medicine Research, Institute for Research and Medical Consultations, Imam Abdulrahman Bin Faisal University, Dammam 31441, Saudi Arabia

* Correspondence: cii_raj@yahoo.com



Citation: Din, S.U.; Kiani, S.H.; Haq, S.; Ahmad, P.; Khandaker, M.U.; Faruque, M.R.I.; Idris, A.M.; Sayyed, M.I. Bio-Synthesized Tin Oxide Nanoparticles: Structural, Optical, and Biological Studies. *Crystals* **2022**, *12*, 614. <https://doi.org/10.3390/cryst12050614>

Academic Editor: Abel Moreno

Received: 1 April 2022

Accepted: 23 April 2022

Published: 26 April 2022

Publisher's Note: MDPI stays neutral with regard to jurisdictional claims in published maps and institutional affiliations.



Copyright: © 2022 by the authors. Licensee MDPI, Basel, Switzerland. This article is an open access article distributed under the terms and conditions of the Creative Commons Attribution (CC BY) license (<https://creativecommons.org/licenses/by/4.0/>).

Abstract: This research was planned to synthesize a biological potent nanomaterials via an eco-friendly process to combat the diseases causing bacteria and the free radicals generated inside the body. For this purpose, a green synthesis process was employed to prepare SnO₂ nanoparticles by utilizing leaf extract of *Populus ciliate*, and they were characterized via different physico-chemical techniques. The crystallite size of SnO₂ nanoparticles was found to be 58.5 nm. The calculated band gap energy of SnO₂ nanoparticles was 3.36 eV. The SnO₂ nanoparticles showed 38, 49, 57, and 72% antioxidant activity at concentrations of 100, 200, 300, and 400 L with 2,2'-azino-bis(3-ethylbenzothiazoline-6-sulfonic acid) (ABTS) assays. The antibacterial effects of prepared SnO₂ nanoparticles were studied using the agar well diffusion method against Gram-positive bacteria (*S. pyogenes* and *S. aureus*) and Gram-negative bacteria (*K. pneumoniae* and *E. coli*). Both the antioxidant activity and antibacterial activity were seen to increase with increasing the concentration of the nanoparticles.

Keywords: *Populus ciliate*; tin dioxide; antioxidant; antibacterial agent

1. Introduction

Bacterial resistance against the antibiotics arises due to their improper use for preventive and corrective purposes without adequate medical indications [1]. Moreover, a lazy lifestyle and carbohydrate-, proteins-, and fats-rich diet of human beings lead to the production of reactive oxygen species (ROS), which produces oxidative stress. Oxidative stress is the reason for degenerative agedness and pathogenesis of different cellular process. It causes cancer, heart, respiratory, and neurodegenerative disease [2]. The high ROS concentration in cells causes ageing, mitochondrial dysfunction, and oxidative stress in the cell [3]. Thus, the bacterial infections and oxidative stress are the two most major risks to public health, and these problems need to be solved to protect human life. The nanotechnology has provided a platform to link different research fields with upgraded outcomes. The nanoparticles (NPs) are mostly used nowadays for antibacterial purpose as a substitute of antibiotics and also as an antioxidant agent [4].

Of the nanoparticles, SnO₂ nanoparticles have gained considerable attention among the several metal oxide semiconductors, as they are highly conducting, transparent, and sensitive to gases [5]. SnO₂ is an n-type semiconductor and has a huge energy spacing of (3.6 eV) [5]. These nanoparticles have a high surface-to-volume ratio, making them potential contenders for acting as free radical scavengers. They are also used as antibacterial agents, as they have the ability to pass the cell membrane readily due to their smaller size; in comparison to traditional medicines, they may transport entire body parts. In many different fields, such as in lithium rechargeable batteries, transparent conducting films, dye-sensitized photovoltaic cells, catalytic materials, environmental monitoring, biochemical sensor, and ultrasensitive gas sensors, SnO₂ nanoparticles are used [6–9]. Most recently, SnO₂ nanoparticles have also been used for their antioxidant and antibacterial potentials. Several chemical and physical approaches have been developed by researchers to synthesize SnO₂ nanoparticles, including hydrothermal, co-precipitation, sol-gel, chemical vapor deposition, carbothermal, and solvothermal processes [10–13]. However, researchers ought to replace these manufacturing techniques with safe, economical, nonpoisonous, and ecologically sustainable green methods because of environmental issues [14]. In the recent past, SnO₂ nanoparticles have been synthesized by using different plants, including *Daphne mucronata*, *Punica grantum*, *Aspalathus linearis*, and *Persia americana* (leaf, root and fruit) extract, and were used for biological and photocatalytic applications [15–18]. Several studies have also been reported on the green synthesis of SnO₂ nanoparticles that have been utilized for the adsorption of heavy metals, photo-reduction of organic dyes, and biological applications [14,15]. However, no literature was found for the *Populus ciliata*-mediated synthesis of SnO₂ nanoparticles. Thus, it is claimed that the present study is novel in the sense that the detailed antibacterial and antioxidant investigation of SnO₂ nanoparticles synthesized using *Populus ciliata* has never been reported before. *Populus ciliata* is commonly known as Himalayan poplar and is a member of family Salicaceae. *Populus ciliata* is composed of the phytochemicals such as proteins, phenolic glycosides, carbohydrates, tannins, flavonoids, saponins, and terpenoids [19]. The leaves are generally utilized as fodder and fuel and are also used to identify and explore genetic diversity [20].

In the current study, the green synthesis route was followed to prepare SnO₂ nanoparticles using *Populus ciliata* extract. The synthesized nanoparticles were characterized by X-ray diffraction (XRD), scanning electron microscopy (SEM), fourier transform infrared spectroscopy (FTIR), energy dispersive X-ray (EDX), diffuse reflectance spectroscopy (DRS), and thermogravimetric analysis (TGA). The antioxidant and antibacterial properties of the synthesized nanoparticles were studied by following ABTS assay and agar well diffusion protocols.

2. Materials and Methods

2.1. Preparation of SnO₂ Nanoparticles

To prepare the extract, leaves of *Populus ciliate* were introduced into 1000 mL of deionized water and boiled in deionized water for three hour. The resulting extract was filtered and stored for further use. Next, 0.25 M SnCl₄·5H₂O (Sigma-Aldrich, St. Louis, MO, USA) solution was added to 20 mL of the prepared extract and heated and stirred at 60 °C for 30 min at its natural pH (2). After that, the solution of sodium hydroxide (Sigma-Aldrich, St. Louis, MO, USA) was gradually added to increase the pH to 10. The obtained white gel was washed with deionized water followed by ethanol (Sigma-Aldrich, St. Louis, MO, USA) and desiccated at 70 °C in the oven and stored in an air-tight vial.

2.2. Characterization

The XRD measurement was carried out using a Panalytical X'pert pro (PW 3040/60) diffractometer in the 2-theta range of 20° to 80°. The surface morphology was examined with a Carl Zeiss supra 40 FESEM model JEOL 5910 (Tokyo, Japan). The percentage composition and purity was analyzed through EDX. The UV-Visible absorption phenomena

was observed during the DRS analysis (Thermo Fisher Scientific, Waltham, MA, USA) and band gap was determined through Tauc plot. The FTIR measurement was carried out with a Shimadzu FTIR spectrophotometer model 8400S (Thermo Fisher Scientific Waltham, MA, USA). The thermal stability was checked during the TGA analysis, where a known quantity of the sample was heated with increasing rate of 10 °C rise per min up to 600 °C.

2.3. Antimicrobial Activity

By agar well diffusion method, the antimicrobial activity of SnO₂ nanoparticles was assessed against two Gram-positive and two Gram-negative bacteria. The bacteria were cultured in nutrient agar. The overnight bacterial culture mixed in freshly prepared, sterilized agar medium was placed in the disinfected Petri plates and enabled to solidify at 25 °C in a laminar flow. The 5 mm diameter wells were created in each plate through the tip of a sterilized micropipette, and a sterilized needle was used to remove the agar plug. Through ultrasonic dispersion, various suspensions of SnO₂ nanoparticles were prepared in DMSO, and these suspensions were put into each well and kept in an incubator overnight at 37 °C. After a day, the inhibition zone was measured in millimeters (mm) across each well to check the activity of SnO₂ nanoparticles [21].

2.4. Antioxidant Activity

The antioxidant capacity of calcined SnO₂ nanoparticles was analyzed using the ABTS radical scavenging assay. When ABTS^{•+}, a radical cation, was reduced to ABTS (2,2'-azino-bis(3-ethylbenzothiazoline-6-sulphonic acid) diammonium salt), decolorization occurred. The ABTS stock solution was produced by mixing 2.5 mM potassium persulphate in 7 mM ABTS. Then, to generate ABTS^{•+} free radicals, the mixture was kept in dark for 16 h. The UV-double-beam spectrophotometer (Shimadzu UV 1800) was utilized to measure the absorbance recorded at 734 nm (A_0). The solution of SnO₂ nanoparticles was obtained by dissolving each calcined sample in dimethyl sulfoxide (DMSO) at 1 mgmL⁻¹ concentration. Then, 1 mL of ABTS^{•+} solution was mixed with SnO₂ nanoparticles in the range of 50–300 µgmL⁻¹ for testing, and the absorbance of the test sample (A_i) was measured at 734 nm. Equation (1) was employed to calculate the percentage radical scavenging activity, where absorbance of control is represented by A_0 , and absorbance of test is A_i . During the experiment, ascorbic acid with the same concentrations was used as a standard.

$$\%RSA = \left[\left(A_0 + A_i / A_0 \right) \right] \times 100 \quad (1)$$

3. Results and Discussion

3.1. XRD Analysis

XRD was employed to examine the crystalline structure of the prepared SnO₂ nanoparticles and the XRD pattern in Figure 1. The XRD peaks observed at 2θ values are 26.68°, 32.77°, 38.24°, 43.88°, 51.84°, 54.71°, 58.49°, 62.14°, 65.58°, 71.29°, 74.44°, and 78.85° with corresponding hkl values of (110), (101), (200), (210), (221), (220), (002), (221), (301), (202), (212), and (321). All of the peaks found are similar to ones mentioned in reference card 01-077-0451 and verify the tetragonal structure of SnO₂ nanoparticles [22]. The length of a and b coordinates is 4.7509 Å, while the c coordinate is 3.1965 Å long. All the three angles (alpha, beta, and gamma) are equal to 90°. The calculated density was found to be 6.93 g/cm³ with total cell volume of 72.15 × 10⁶ pm³. The origin software was used to determine the crystallinity of SnO₂ nanoparticles and was found to be 87.62%. Debye Scherer's equation was used to determine the crystallite size:

$$D = \frac{k\lambda}{\beta \cos\theta} \quad (2)$$

where the crystallite size is represented by D , k is the shape factor constant whose value varies from 0.89 to 1, λ is the X-ray radiation wavelength (0.1546 nm), β represents the FWHM, and θ is Bragg's diffraction angle. The lattice constant a is determined through the following equation and the data obtained is listed in Table 1.

$$a = d_{hkl} (h^2 + k^2 + l^2)^{1/2} \quad (3)$$

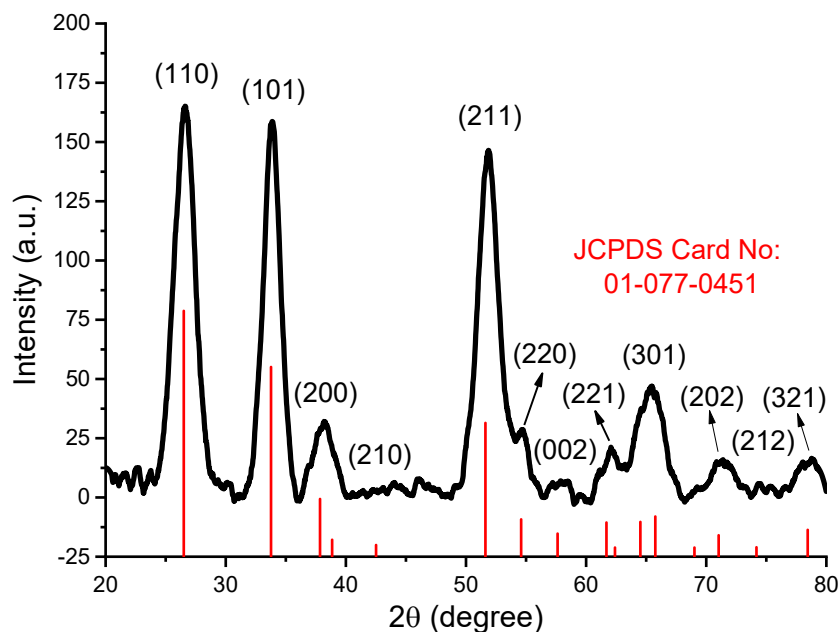


Figure 1. X-ray diffractogram of SnO₂ nanoparticles.

Table 1. Calculated interplanar spaces (d) and lattice constant (a).

Miller Indices (hkl)	2θ Values	d (Å)	a (Å)
110	26.68°	0.344	0.486
101	32.77°	0.285	0.403
200	38.24°	0.250	0.5
211	51.84°	0.196	0.480
221	62.14°	0.174	0.522
301	65.58°	0.169	0.534
202	71.29°	0.163	0.461
321	78.85°	0.157	0.608

Where a represents the lattice constant and h , k , and l are the Miller indices. The calculated crystallite size of SnO₂ nanoparticles is 10 nm, while the lattice strain of crystal is 0.345 percent.

3.2. SEM Analysis

SEM technique was used to examine the morphology of the obtained SnO₂ nanoparticles. The SEM micrographs of SnO₂ nanoparticles are depicted in Figure 2. These micrographs demonstrate the cluster-like structure of SnO₂ nanoparticles. They all are highly agglomerated nanoparticles with no specific form or geometry. The measured diameter size varies from 48.4 nm to 100 nm, and their average size is 75.5 nm [23].

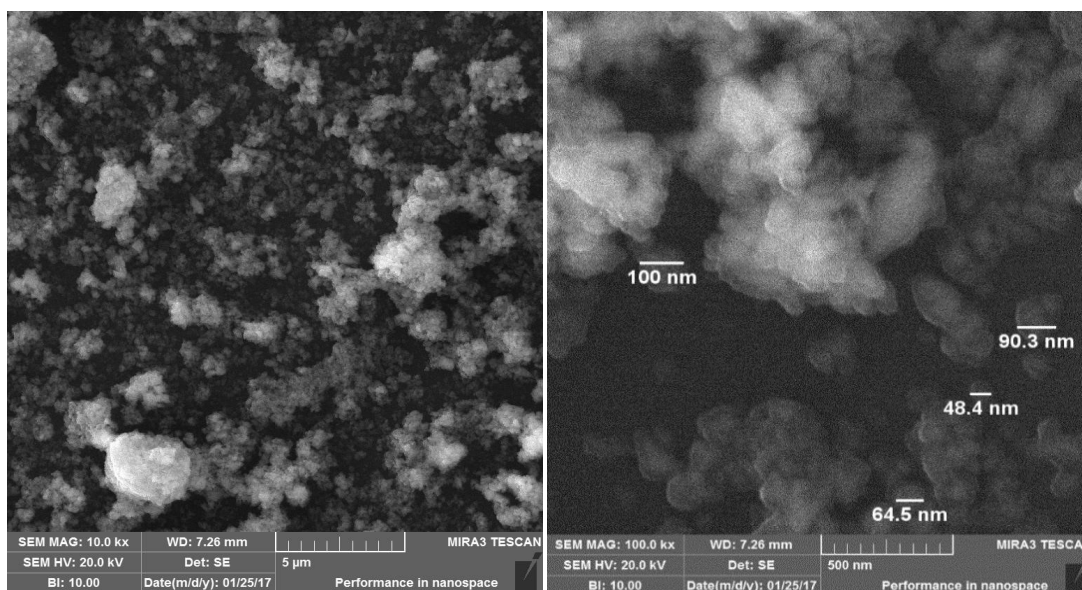


Figure 2. SEM image of SnO₂ nanoparticles.

3.3. FTIR Analysis

The functional group of obtained nanoparticles are determined by FTIR analysis. Figure 3 illustrates the FTIR spectrum of SnO₂ nanoparticles. The first absorption band is seen in the range of 3471 to 3031 cm⁻¹, which indicates the existence of O–H group due to the absorbed water molecules at SnO₂ surface as well as the Sn–OH groups' stretching vibration [18]. The second peak at 1620 cm⁻¹ is for the bending vibration of –OH group. The third peak at 1375 cm⁻¹ is observed due to COOH group, which is approximately similar to the peak at 1395 cm⁻¹ that is mentioned in past work. The next peak at 1152 cm⁻¹ Sn–OH is for the stretching vibration, whereas the peaks at 1076 and 1027 cm⁻¹ are attributed to the stretching vibration of C–O, which is similar to the literature [24]. The absorption band at 768 to 482 cm⁻¹ represents the different Sn–O or Sn=O stretching modes [25].

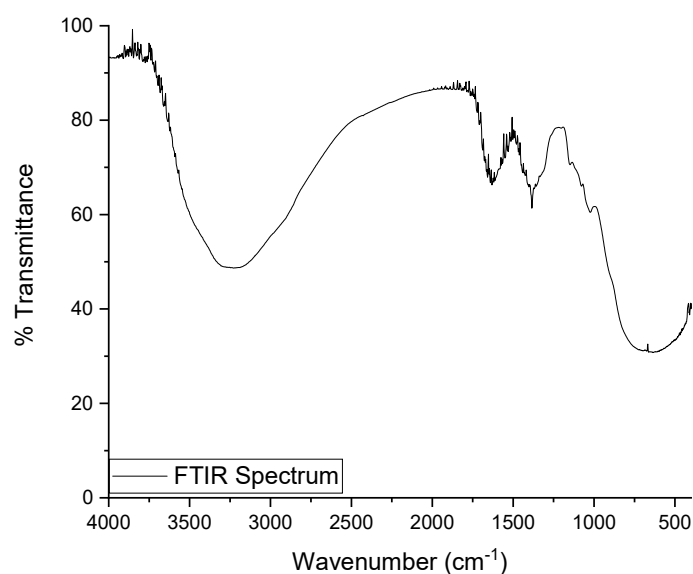


Figure 3. FTIR spectrum of SnO₂ nanoparticles.

3.4. DRS Analysis

Diffused reflectance spectroscopy and Tauc plot were utilized to evaluate the optical band gap of nanoparticles. Figure 4a showed the DRS spectrum of SnO₂ nanoparticles. The transmittance edge wavelength was obtained by combining the sharp elevation region of UV-VIS curve with DRS spectrum's X-axis [26]. For SnO₂ nanoparticles, the transmittance edge of 500 nm is seen in the visible region of DRS spectrum from where transmittance increased gradually, while absorbance is decreased. Figure 4b represented the Tauc plot for SnO₂ nanoparticles. The Tauc model equation to calculate the band gap energy is given as:

$$\alpha h\nu = A (h\nu - E_g)^{n/2} \quad (4)$$

where α represents the linear absorption coefficient, h is the Planck's constant, ν is the light frequency, A is the constant, and E_g is the band gap energy of substance whose values are shown in Table 2. The n is an exponent that relies upon the type of semiconductor band transition. For directly allowed or forbidden and indirectly allowed or indirectly forbidden transition, the n values are 1, 2, 3, and 4, respectively. Using the above Equation (4), the band gap energy of SnO₂ nanoparticles was determined to be 3.36 eV, which is in good accord with the past literature value [27].

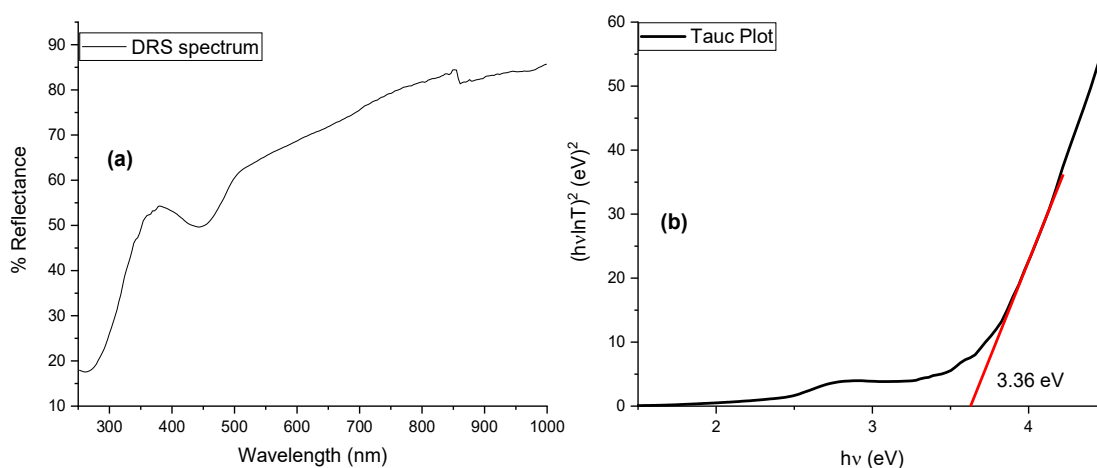


Figure 4. DRS spectrum (a) Tauc plot (b) for SnO₂ nanoparticles.

Table 2. Optical band gap energy of SnO₂ nanoparticles.

Planck's Constant (h)	Velocity of Light (c)	Band Gap Reflectance Edge (λ)	Optical Band Gap Energy (E_g)
$6.626 \times 10^{-34} \text{ J s}$	$3 \times 10^8 \text{ m s}^{-1}$	500 nm	3.36 eV

3.5. EDX Analysis

EDX analysis was employed for the elemental detection and quantitative details. Figure 5 represents the EDX spectrum of SnO₂ nanoparticles. The peaks related to the O and Cl are present at 0.2 keV and 2.2 keV, whereas the sharp peaks at 3.1 keV and 4.1 keV are due to the existence of Sn in the sample. EDX spectrum also revealed the presence of C in the sample that could be due to the used plant extract or carbon tap, while the presence of chlorine in the sample is due to the used SnCl₄·5H₂O salt. The weight percentage determined by EDX analysis of Sn, O, and Cl are 74.0, 19.9, and 6.1%, respectively.

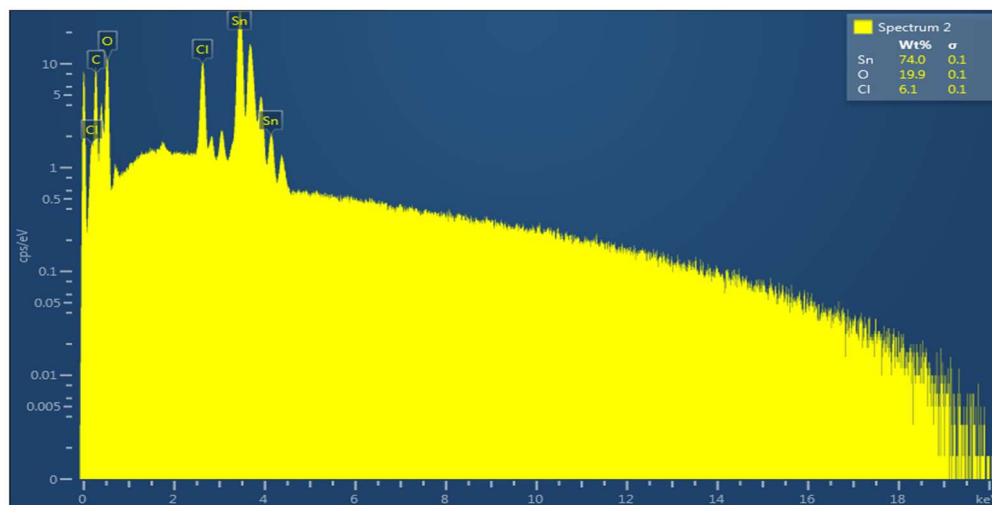


Figure 5. EDX spectrum of SnO₂ nanoparticles.

3.6. TGA Analysis

TGA analysis was employed for thermal observation of prepared SnO₂ nanoparticles. Two weight losses are noticed on the thermogram (Figure 6) of SnO₂ nanoparticles. The initial weight of the sample is 25.50 mg and the first weight loss of 0.03 mg occurred in the range 40–245 °C, which may be caused by evaporation of ethanol traces and adsorbed moisture. The second weight loss of 0.18 mg is observed at 246–530 °C, which is most probably due to the decomposition of the coordinated biomolecules (from plant source), and condensation Sn–OH surface group into SnO₂ (elimination of chemical bonded water molecule) led to the reduction in weight to 25.29 mg. After 530 °C, the sample weight remained almost constant, and a very slight weight loss of 0.9% is observed in the sample, which is approximately 0.21 mg [28]. TGA data of synthesized SnO₂ nanoparticles are shown in Table 3.

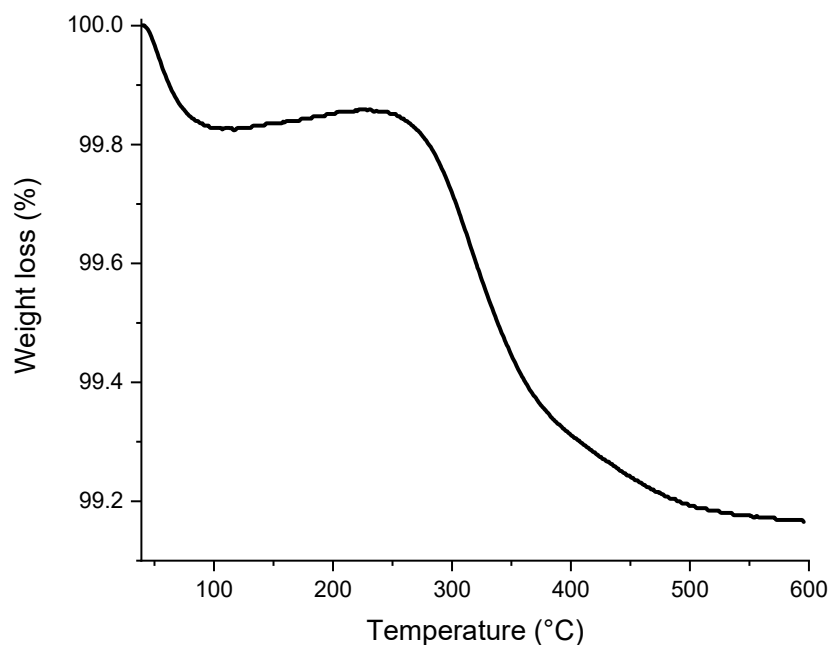


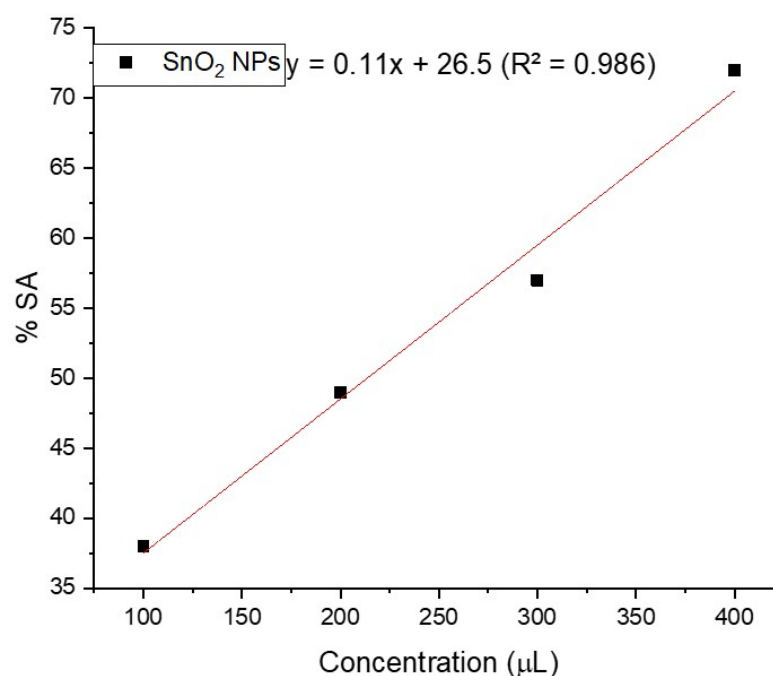
Figure 6. TGA of SnO₂ nanoparticles.

Table 3. TGA data of synthesized SnO₂ nanoparticles.

Stages	Temperature (°C)	Weight Loss (mg)	Total Weight Loss
1st	40–245 °C	0.03 mg	0.21 mg
2nd	246–530 °C	0.18 mg	
3rd	After 530 °C	No weight loss	

3.7. Antioxidant Property

The antioxidant activity of the prepared SnO₂ nanoparticles is investigated by ABTS free radical scavenging activity, which decolorizes when scavenged. Figure 7 depicts the percentage scavenging activity with regard to sample concentration. The antioxidant performance is increased with the rise in sample concentration, as illustrated in Table 4. The amount of reactive species is increased with SnO₂ nanoparticles concentration, and therefore, the ability of sample to combat the reactive ABTS^{•+} free radical is also increased, increasing the radical scavenging capacity of SnO₂ nanoparticles [29]. The calculated IC₅₀ value is 213.64, which is closer to the value reported elsewhere [30].

**Figure 7.** Antioxidant activity of SnO₂ nanoparticles against ABTS free radicals.**Table 4.** Antioxidant activity values of different samples of SnO₂ nanoparticles.

Samples Code	Concentration (µL)	Percentage Scavenging Activity (%)	IC ₅₀
SnO ₂ nanoparticles	100	38	213.64
	200	49	
	300	57	
	400	72	

3.8. Antimicrobial Activity

SnO₂ nanoparticles are tested for antimicrobial activity against Gram-positive bacteria *S. pyogenes* and *S. aureus* as well as Gram-negative *K. pneumoniae* and *E. coli* bacteria. Figure 8 depicts the experimental images of antibacterial activity of SnO₂ nanoparticles. The activity generated millimeter-sized inhibition zones. Table 4 illustrates that the antimicrobial activity of nanoparticles is increased by increasing the volume of suspension

of SnO₂ nanoparticles in wells. This is because of the reduced size and larger surface area of SnO₂ nanoparticles, which led to the production of abundant tin cation, which in turn has potential to inhibit significant number of bacterial species. In contrast to Gram-negative bacteria, Gram-positive bacteria *S. pyogenes* and *S. aureus* are more resistant to SnO₂ nanoparticles. The antimicrobial action of SnO₂ nanoparticles differed owing to variation in surface electrostatic force, cell wall composition, and structure [31]. The thick peptidoglycan layer is found in the Gram-positive bacteria cell wall, which make it difficult for SnO₂ nanoparticles to penetrate, resulting in low activity, while the presence of phospholipids and lipopolysaccharides results in a high negative-charge surface of the Gram-negative bacteria. Unlike Gram-positive bacteria, Gram-negative bacteria showed highest activity because of the significant association of Sn²⁺ with strong negative charge. As a result, a higher concentration of Sn²⁺ accumulates on the surface of Gram-negative bacteria, initiating cell bursting and also allowing easy permeation within the cells [32,33].

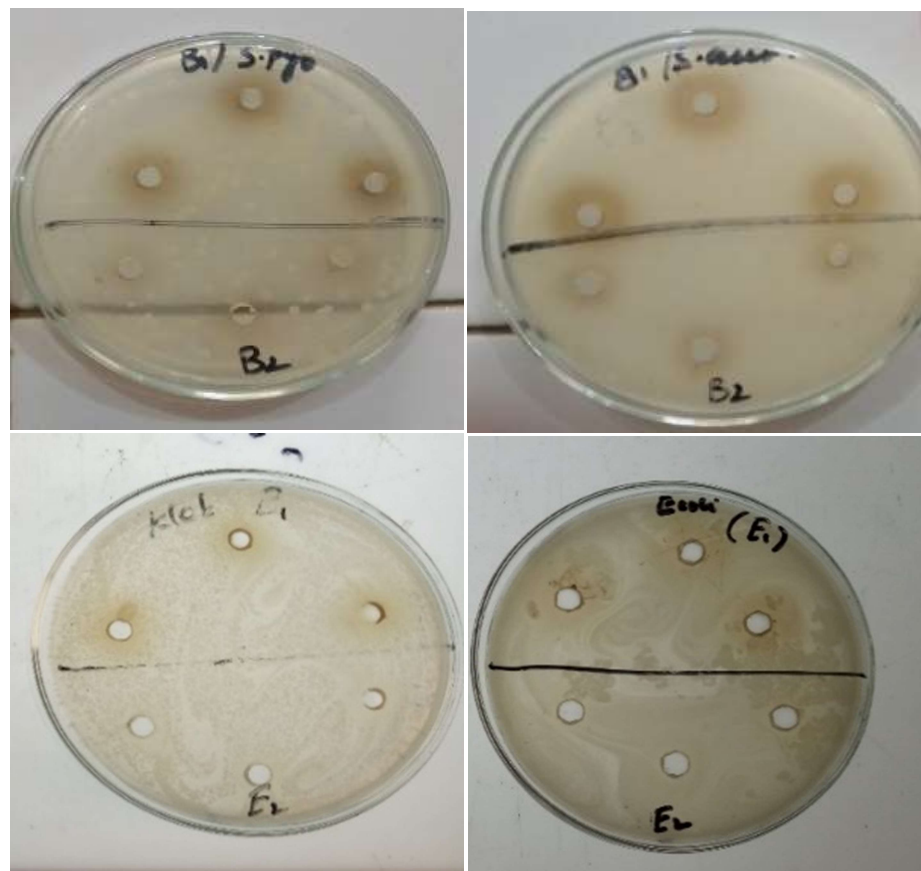


Figure 8. Experimental photographs of antibacterial activity of SnO₂ nanoparticles against Gram-positive and Gram-negative bacteria.

Metal oxide nanoparticles have a different antimicrobial mechanism. Hydroxyl radicals, metal cation, and super oxide radical anions are formed in aqueous suspensions of SnO₂ nanoparticles [15,34]. Metallic oxides release metal ions, which combine with the thiol group of a bacterial enzyme, inactivating it and causing cell death, or as light interacts with the surface of SnO₂ nanoparticles, electrons are excited, which form oxygen ions by reacting with absorbed oxygen, which then react with H₂O molecules to form hydrogen peroxide. The H₂O₂ then enter into the bacterial cell, disrupt the cytoplasmic composition, and ultimately kill the bacteria [35].

4. Conclusions

The tetragonal-shaped SnO₂ nanoparticles were successfully synthesized by a simple and economical process, where the *Populus ciliata* leaf extract was used as a reducing agent. The apparent structure and size of the nanoparticles are not uniform, which might be due to rapid precipitation of the sample. The FTIR and TGA results confirm the presence of a hydroxyl group in the sample. The calculated band gap energy is less than the one reported in literature, which might be to the larger size of the SnO₂ nanoparticles. The ABTS scavenging activity is found to increase with increasing the concentration of the sample in the reaction, and maximum activity was at a higher concentration. A similar pattern was also seen in the antibacterial activity, and the gradual increase in the activity was observed with increasing concentration of the sample. In the future, the synthesized SnO₂ nanoparticles can be utilized as photocatalysts, biochemical sensors, and in solar cell formation.

Author Contributions: Conceptualization, S.H. and S.U.D.; methodology, S.H.K. and A.M.I.; software, S.H. and M.U.K.; validation, P.A., M.U.K. and M.I.S.; formal analysis, S.H.K.; investigation, S.H., P.A. and A.M.I.; resources, S.U.D., M.U.K. and M.R.I.F.; data curation, M.I.S. and P.A.; writing—original draft preparation, S.H.K. and M.R.I.F.; writing—review and editing, S.H., M.U.K., A.M.I. and S.U.D.; visualization, P.A. and S.H.; supervision, S.U.D.; project administration, M.I.S. and S.H.; funding acquisition, M.I.S., M.R.I.F. and A.M.I. All authors have read and agreed to the published version of the manuscript.

Funding: The authors extend their appreciation to the Deputyship for Research & Innovation, Ministry of Education in Saudi Arabia for funding this research work through the project number IFP-KKU-2020/4.

Data Availability Statement: All the data is available within the manuscript.

Conflicts of Interest: The authors declare no conflict of interest.

References

1. Hajipour, M.J.; Fromm, K.M.; Ashkarran, A.A.; Jimenez de Aberasturi, D.; de Larramendi, I.R.; Rojo, T.; Serpooshan, V.; Parak, W.J.; Mahmoudi, M. Antibacterial properties of nanoparticles. *Trends Biotechnol.* **2012**, *30*, 499–511. [[CrossRef](#)] [[PubMed](#)]
2. Ahmad, W.; Kalra, D. Green synthesis, characterization and antimicrobial activities of ZnO nanoparticles using Euphorbia hirta leaf extract. *J. King Saud Univ.-Sci.* **2020**, *32*, 2358–2364. [[CrossRef](#)]
3. Liew, S.S.; Ho, W.Y.; Yeap, S.K.; Bin Sharifudin, S.A. Phytochemical composition and in vitro antioxidant activities of Citrus sinensis peel extracts. *PeerJ* **2018**, *2018*, e5331. [[CrossRef](#)]
4. Din, M.I.; Arshad, F.; Hussain, Z.; Mukhtar, M. Green Adeptness in the Synthesis and Stabilization of Copper Nanoparticles: Catalytic, Antibacterial, Cytotoxicity, and Antioxidant Activities. *Nanoscale Res. Lett.* **2017**, *12*, 638. [[CrossRef](#)]
5. Drzymala, E.; Gruzal, G.; Depciuch, J.; Budziak, A.; Kowal, A.; Parlinska-Wojtan, M. Structural, chemical and optical properties of SnO₂ NPs obtained by three different synthesis routes. *J. Phys. Chem. Solids* **2017**, *107*, 100–107. [[CrossRef](#)]
6. PMahfooz-ur-Rehman; Waseem, M.; Rehman, W.; Hussain, R.; Hussain, S.; Haq, S.; Anis-ur-Rehman, M. Evaluation of structural, electrical and magnetic properties of nanosized unary, binary and ternary particles of Fe₃O₄, SnO₂ and TiO₂. *Chem. Pap.* **2021**, *75*, 2625–2638. [[CrossRef](#)]
7. Bibi, N.; Haq, S.; Rehman, W.; Waseem, M.; Rehman, M.U.; Shah, A.; Khan, B.; Rasheed, P. Low temperature fabrication of SnO₂, ZnO and Zn₂SnO₄ nanostructures for the degradation of Rhodamine 6G: Characterization. *Biointerface Res. Appl. Chem.* **2020**, *10*, 5895–5900.
8. Naje, A.N.; Norry, A.S.; Suhail, A.M. Preparation and Characterization of SnO₂ Nanoparticles. *Int. J. Innov. Res. Sci. Eng. Technol.* **2013**, *2*, 7068–7072. [[CrossRef](#)]
9. Pereira, M.S.; Ribeiro, T.S.; Lima, F.A.S.; Santos, L.P.M.; Silva, C.B.; Freire, P.T.C.; Vasconcelos, I.F. Synthesis and properties of Sn_{1-x}FexO₂ nanoparticles obtained by a proteic sol-gel method. *J. Nanoparticle Res.* **2018**, *20*, 212. [[CrossRef](#)]
10. Aziz, M.; Saber Abbas, S.; Wan Baharom, W.R. Size-controlled synthesis of SnO₂ nanoparticles by sol-gel method. *Mater. Lett.* **2013**, *91*, 31–34. [[CrossRef](#)]
11. Rahmi, R.; Kurniawan, F. Synthesis of SnO₂ Nanoparticles by high potential electrolysis. *Bull. Chem. React. Eng. Catal.* **2017**, *12*, 281–286. [[CrossRef](#)]
12. Leite, E.R.; Gomes, J.W.; Oliveira, M.M.; Lee, E.J.; Longo, E.; Varela, J.A.; Paskocimas, C.A.; Boschi, T.M.; Lanciotti, J.F.; Pizani, P.S.; et al. Synthesis of SnO₂ nanoribbons by a carbothermal reduction process. *J. Nanosci. Nanotechnol.* **2002**, *2*, 125–128. [[CrossRef](#)]

13. Masuda, Y.; Ohji, T.; Kato, K. Highly enhanced surface area of tin oxide nanocrystals. *J. Am. Ceram. Soc.* **2010**, *93*, 2140–2143. [[CrossRef](#)]
14. Haq, S.; Rehman, W.; Waseem, M.; Shahid, M.; Rehman, M.U.; Shah, K.H.; Nawaz, M. Adsorption of Cd²⁺ ions on plant mediated SnO₂ nanoparticles. *Mater. Res. Express* **2016**, *3*, 105019. [[CrossRef](#)]
15. Haq, S.; Rehman, W.; Waseem, M.; Shah, A.; Khan, A.R. Green synthesis and characterization of tin dioxide nanoparticles for photocatalytic and antimicrobial studies. *Mater. Res. Express* **2020**, *7*, 025012. [[CrossRef](#)]
16. Singh, J.; Kaur, H.; Kukkar, D.; Mukamia, V.K.; Kumar, S.; Rawat, M. Green synthesis of SnO₂ NPs for solar light induced photocatalytic applications. *Mater. Res. Express* **2019**, *6*, 115007. [[CrossRef](#)]
17. Diallo, A.; Manikandan, E.; Rajendran, V.; Maaza, M. Physical & enhanced photocatalytic properties of green synthesized SnO₂ nanoparticles via *Aspalathus linearis*. *J. Alloys Compd.* **2016**, *681*, 561–570. [[CrossRef](#)]
18. Elango, G.; Kumaran, S.M.; Kumar, S.S.; Muthuraja, S.; Roopan, S.M. Green synthesis of SnO₂ nanoparticles and its photocatalytic activity of phenolsulfonphthalein dye. *Spectrochim. Acta-Part A Mol. Biomol. Spectrosc.* **2015**, *145*, 176–180. [[CrossRef](#)]
19. Haq, F.; Ahmad, H.; Alam, M. Traditional uses of medicinal plants of Nandiar Khuwarr catchment (District Battagram), Pakistan. *J. Med. Plants Res.* **2011**, *5*, 39–48.
20. Aggarwal, G.; Gaur, A.; Srivastava, D.K. Establishment of high frequency shoot regeneration system in Himalayan poplar (*Populus ciliata* Wall. ex Royle) from petiole explants using Thidiazuron cytokinin as plant growth regulator. *J. For. Res.* **2015**, *26*, 651–656. [[CrossRef](#)]
21. Haq, S.; Rehman, W.; Waseem, M.; Meynen, V.; Ullah, S.; Saeed, S.; Iqbal, N. Fabrication of pure and moxi fl oxacin functionalized silver oxide nanoparticles for photocatalytic and antimicrobial activity. *J. Photochem. Photobiol. B Biol.* **2018**, *186*, 116–124. [[CrossRef](#)] [[PubMed](#)]
22. Elhaddad, E.; Rehman, W.; Waseem, M.; Nawaz, M.; Haq, S.; Guo, C.Y. Fabrication of Highly Efficient Bi₂Sn₂O₇/C₃N₄ Composite with Enhanced Photocatalytic Activity for Degradation of Organic Pollutants. *J. Inorg. Organomet. Polym. Mater.* **2020**, *31*, 172–179. [[CrossRef](#)]
23. Fu, L.; Zheng, Y.; Ren, Q.; Wang, A.; Deng, B. Green biosynthesis of SnO₂ nanoparticles by plectranthus amboinicus leaf extract their photocatalytic activity toward rhodamine B degradation. *J. Ovonic Res.* **2015**, *11*, 21–26.
24. Ho, S.Y.; Wong, A.S.W.; Ho, G.W. Controllable porosity of monodispersed tin oxide nanospheres via an additive-free chemical route. *Cryst. Growth Des.* **2009**, *9*, 732–736. [[CrossRef](#)]
25. Haq, S.; Ahmad, P.; Khandaker, M.U.; Faruque, M.R.I.; Rehman, W.; Waseem, M.; Din, S.U. Antibacterial, antioxidant and physicochemical investigations of tin dioxide nanoparticles synthesized via microemulsion method. *Mater. Res. Express* **2021**, *8*, 035013. [[CrossRef](#)]
26. Shoukat, S.; Haq, S.; Rehman, W.; Waseem, M.; Shahzad, M.I.; Shahzad, N.; Hafeez, M.; Din, S.U.; Zain-ul-Abdin; Shah, A.; et al. Fabrication and Characterization of Zinc Titanate Heterojunction for Adsorption and Photocatalytic Applications. *J. Inorg. Organomet. Polym. Mater.* **2020**, *30*, 4944–4953. [[CrossRef](#)]
27. Haq, S.; Rehman, W.; Waseem, M.; Rehman, M.U.; Khan, B. Adsorption of Cd²⁺ ions onto SnO₂ nanoparticles synthesized via sol-gel method: Physicochemical study. *Mater. Res. Express* **2019**, *6*, 105035. [[CrossRef](#)]
28. de Monredon, S.; Cellot, A.; Ribot, F.; Sanchez, C.; Armelao, L.; Gueneau, L.; Delattre, L. Synthesis and characterization of crystalline tin oxide nanoparticles. *J. Mater. Chem.* **2002**, *12*, 2396–2400. [[CrossRef](#)]
29. Haq, S.; Dildar, S.; Ali, M.B.; Mezni, A.; Hedfi, A.; Shahzad, M.I.; Shahzad, N.; Shah, A. Antimicrobial and antioxidant properties of biosynthesized of NiO nanoparticles using Raphanus sativus (R. sativus) extract. *Mater. Res. Express* **2021**, *8*, 055006. [[CrossRef](#)]
30. Rehman, F.U.; Mahmood, R.; Ali, M.B.; Hedfi, A.; Mezni, A.; Haq, S.; Din, S.U.; Ehsan, R. Physicochemical, Photocatalytic, Antibacterial, and Antioxidant Screening of Bergenia Ciliata Mediated Nickel Oxide Nanoparticles. *Crystal* **2021**, *11*, 1137. [[CrossRef](#)]
31. Haq, S.; Yasin, K.A.; Rehman, W.; Waseem, M.; Ahmed, M.N.; Shahzad, M.I.; Shahzad, N.; Shah, A.; Rehman, M.U.; Khan, B. Green Synthesis of Silver Oxide Nanostructures and Investigation of Their Synergistic Effect with Moxifloxacin Against Selected Microorganisms. *J. Inorg. Organomet. Polym. Mater.* **2020**, *31*, 1134–1142. [[CrossRef](#)]
32. Precious Ayanwale, A.; Reyes-López, S.Y. ZrO₂-ZnO Nanoparticles as Antibacterial Agents. *ACS Omega* **2019**, *4*, 19216–19224. [[CrossRef](#)] [[PubMed](#)]
33. Shah, A.; Haq, S.; Rehman, W.; Muhammad, W.; Shoukat, S.; Rehman, M.U. Photocatalytic and antibacterial activities of Paeonia emodi mediated silver oxide nanoparticles. *Mater. Res. Express* **2019**, *6*, 045045. [[CrossRef](#)]
34. Hamid, A.; Haq, S.; Ur Rehman, S.; Akhter, K.; Rehman, W.; Waseem, M.; Ud Din, S.; Zain-ul-Abdin; Hafeez, M.; Khan, A.; et al. Calcination temperature-driven antibacterial and antioxidant activities of fumaria indica mediated copper oxide nanoparticles: Characterization. *Chem. Pap.* **2021**, *75*, 4189–4198. [[CrossRef](#)]
35. Haq, S.; Rehman, W.; Waseem, M.; Javed, R.; Mahfooz-ur-Rehman; Shahid, M. Effect of heating on the structural and optical properties of TiO₂ nanoparticles: Antibacterial activity. *Appl. Nanosci.* **2018**, *8*, 11–18. [[CrossRef](#)]